Qualitative and Quantitative Structure−Property Relationships Analysis of Multicomponent Potential Bioglasses

Laura Linati,[†] Gigliola Lusvardi,[‡] Gianluca Malavasi,[‡] Ledi Menabue,*[,‡] M. Cristina Menziani,*[,‡] Piercarlo Mustarelli,[§] and Ulderico Segre[‡]

Centro Grandi Strumenti, University of Pavia, Via Bassi 21, 27100 Pavia, Italy, Department of Chemistry and SCS center, University of Modena and Reggio Emilia, Via G.Campi 183, 41100 Modena, Italy, and Department of Physical Chemistry "M. Rolla", University of Pavia, and IENI-CNR, Via Taramelli 16, 27100 Pavia, Italy

Received: July 28, 2004; In Final Form: October 12, 2004

The results of a qualitative and quantitative structure−property relationships analysis of multicomponent potential bioglasses of composition $(2 - y)SiO_2 \cdot 1Na_2O \cdot 1.1CaO \cdot yP_2O_5 \cdot xZnO$ ($x = 0$, 0.16, 0.35, 0.78 and $y = 0.10$, 0.20, 0.36) are presented. Quantitative models are obtained by means of structural descriptors derived by molecular dynamics simulations and experimental data measured for density, thermal analysis, ^{29}Si and ^{31}P magic angle spinning NMR, and chemical durability in water. Analysis of the crystal species obtained upon glass crystallization helped in the rationalization of the structural role of the different components. Finally, glass surface characterization with scanning electron microscopy, transmission electron micrsocopy, and X-ray diffraction after soaking in acellular simulated body fluid demonstrated the in vitro bioactivity of the newly obtained $1.80SiO_2 \cdot 1Na_2O \cdot 1.1Ca \cdot 0.20P_2O_5 \cdot 0.16ZnO$ (HP5Z5) glass, corresponding to $x = 0.16$ and $y = 0.20$.

Introduction

Bioactive glasses are widely used clinically in the repair of bone defects[1] because they spontaneously bond and integrate with bone in the living body through the rapid formation of a thin hydroxy-carbonate-apatite layer on the surface of the material, when implanted or in contact with biological fluids.[2] Since the early 1970s, when the first Bioglass (45S5 glass: 24.5% Na_2O−24.5% CaO−45.0% SiO_2−6% P_2O_5 by weight) was synthesized,[2] glasses of many different compositions have been studied to improve the mechanical strength up to a level comparable to cortical bone, thus, overcoming the most severe limiting factor in medical use. By varying the chemical nature and concentration of dopants, new important biological properties (i.e., bacteriostatic, cariostatic, etc.) can also be added and the glass can be tailored to specific clinical applications.

It has recently been demonstrated that zinc, an essential trace element, manifests stimulatory effects on bone formation in vitro and in vivo. In fact, the slow release of zinc incorporated into an implant material promotes bone formation around the implant and accelerates recovery of the patient.[3] Moreover, it is well-known that zinc addition to silicate and borosilicate glasses improves the thermal and mechanical properties[4,5] and brings acceptable aqueous durability in phosphate glasses.[6]

Therefore, Bioglass 45S5 doped with zinc should show a reinforced structure and a promoting effect on tissue regeneration. However, optimization of the composition is required to obtain glasses with preserved bioactivity, apatite forming ability, and an optimal zinc oxide releasing rate.

In general, a useful tool for the optimization of the final properties of a set of chemical objects is the theoretical quantitative structure−property relationships (QSPR) analysis. This technique, which has a corollary in drug design,[7] relates properties to numerical representations of structures through mathematical models, thus, assuming an immense practical importance in the development of predictive and interpretative models. However, its application in the field of material design is still at dawn.[8]

We present in this paper the results of a QSPR analysis of Zn-doped glasses based on the Bioglass 45S5 composition. Theoretical structural descriptors derived from molecular dynamics (MD) simulations have been utilized to rationalize, in a quantitative way, the variation of experimental data measured for density, thermal analysis, ^{29}Si and ^{31}P magic angle spinning (MAS) NMR, and chemical durability in water.

The formulation of informative QSPR models adequate for multicomponent disordered systems is anything but trivial, and to our knowledge, this is the first time in which a theoretical QSPR approach has been applied to the field of inorganic glasses.

MD computer simulations allow the investigation of glass structure at the atomistic level of detail and constitute an efficient and relatively inexpensive tool to unreveal the structure−property relationships in complex real materials. Nevertheless, modeling of the phosphorus' properties is difficult because of the anisotropy of its tetrahedrally hybridized orbitals, and only a limited number of MD simulations on this element have been reported in the literature. In fact, while there are a few studies on zinc phosphate glasses,[9−11] to our knowledge, only one report concerns the Bioglass composition.[12] However, to date no atomistic simulation studies have been carried out on glass systems which contain three different ions with network-forming ability, such as Si, P, and Zn.

* Corresponding authors. E-mail: menabue@unimo.it (L.M.); menziani@unimo.it (M.C.M.). Tel.: +39 059 2055042 (L.M.); +39 059 2055091 (M.C.M.). Fax: +39 059 373543 (L.M.); +39 059 373543 (M.C.M.).

[†] Centro Grandi Strumenti, University of Pavia.

[‡] University of Modena and Reggio Emilia.

[§] Department of Physical Chemistry "M. Rolla", University of Pavia, and IENI-CNR.

10.1021/jp046631n CCC: $30.25
Published on Web 02/24/2005

TABLE 1: Batch Compositions (mol %) from the General Glass Formula $(2 - y)SiO_2 \cdot 1Na_2O \cdot 1.1CaO \cdot yP_2O_5 \cdot xZnO$

			% mol				
glass	x	y	SiO_2	Na_2O	CaO	P_2O_5	ZnO
H	0	0.10	46.2	24.3	26.9	2.6	
HZ5	0.16	0.10	44.4	23.4	25.9	2.5	3.8
HZ10	0.32	0.10	42.5	22.5	24.8	2.4	7.8
HZ20	0.78	0.10	38.8	20.5	22.6	2.2	15.9
HP5	0	0.20	43.7	24.4	26.9	5.0	
HP5Z5	0.16	0.20	42.1	23.4	25.9	4.7	3.9
HP8	0	0.36	40.0	24.4	26.9	8.7	

Therefore, by considering the complexity of the multicomponent systems under investigation and the impact of the force fields used in the MD calculations on the final atomic arrangement obtained, extensive comparisons with the experimental data available in the literature and/or derived in this study from the analysis of the crystal species separated from the glasses have been used to provide conviction on the reliability of the structural models obtained. The use of a quantitative approach renders the results obtained sounder, furnishing elements for the interpretation of the structural role of the different constituents on in vitro bioactivity, evaluated on the basis of the behavior of powder glasses after soaking in acellular simulated body fluid (SBF).

Experimental Section

Glass Preparation. We have synthesized two new series of glasses with the following composition: $(2 - y)SiO_2 \cdot 1Na_2O \cdot 1.1CaO \cdot yP_2O_5 \cdot xZnO$. In the first series ZnO was added, to the base glass 45S5 Bioglass ($x = 0$ and $y = 0.10$, hereafter H), at molar concentrations of 3.8% ($x = 0.16$, hereafter HZ5), 7.8% ($x = 0.35$, hereafter HZ10), and 15.9% ($x = 0.78$, hereafter HZ20). The second series of glasses was more phosphorus-rich. HP5 ($x = 0$, $y = 0.20$) and HP8 ($x = 0$, $y = 0.36$) were prepared by substituting P_2O_5 for SiO_2, and the glass HP5Z5 ($x = 0.16$, $y = 0.20$) was obtained by adding 3.9 mol % of ZnO at the HP5 composition.

The H glass was modified also by addition of 3.8 mol % (HCo5) and 7.8 mol % (HCo10) CoO. The reagents and experimental conditions for the batch preparations were reported previously.[5] P_2O_5 was added as mixture of $Na_3PO_4 \cdot 12H_2O$ and $NaH_2PO_4 \cdot H_2O$, and CoO was added as $CoCO_3$. The heating rates to T maximum (1600 °C) were 5 °C/min (20−500 °C), 10 °C/min (500−1000 °C), and 15 °C/min (>1000 °C); the soaking time at T_{max} was in the range of 1−3 h. The melts were poured into a graphite mold after being ball-milled in agate mill jars and sieved to produce particle size ranges of 108−125 μm for the measurements on powdered glass and 250−500 μm for soaking in SBF. The samples were obtained as transparent homogeneous glasses, while HP8 showed an opaque effect due to partial crystallization.

Rectangular slabs of 1 mm of thickness were made for chemical durability measurements. The molar compositions of the examined glasses are listed in Table 1.

Glass Characterization. Density was determined with a picnometer (Micromeritics, Accupyc 1330) at room temperature with an accuracy of 0.002 g/cm^3. Each value is an average of three independent measurements.

Differential scanning calorimetry measurements were performed in air with a NETZSCH DSC 4 instrument by using ≈30 mg of sample previously finely milled to the 108−125 μm particle size range; the scan rate was 10 °C/min, and the temperature range was 25−1400 °C.

X-ray diffraction (XRD) analysis was performed on the as-quenched glasses, after their thermal treatment (2 h and 30 min or 5 h) and after SBF soaking (15−30 days), with a Philips PW3710-based automated diffractometer, using Ni-filtered Cu Kα radiation ($\lambda = 1.540\,60$ Å). The conditions for data collections were $5 < 2\theta < 60°$ range, with a time step of 8 s and a step size 0.03°.

UV−vis analysis was carried out on finely powdered glasses HCo5 and HCo10 with a Perkin-Elmer Lambda 19 UV−vis instrument in the 190−1100 nm range with $BaSO_4$ as the blank reference.

The MAS NMR measurements were performed at room temperature on a AMX400WB FFT spectrometer (Bruker, Karlsruhe) equipped with 4 and 7 mm MAS probes. The ^{29}Si ($I = 1/2$) spectra were acquired at a Larmor frequency of 79.49 MHz, by rotating the sample at 5 kHz, with a single-pulse sequence (90° pulse = 8 μs, repetition delay = 30 s, spectral width = 100 kHz). About 4000 acquisitions were averaged to obtain an acceptable signal-to-noise ratio. The ^{31}P ($I = 1/2$) spectra were acquired at a Larmor frequency of 161.98 MHz, by rotating the sample at 12 kHz, with a single-pulse sequence (10° pulse = 0.7 μs, repetition delay = 60 s, spectral width = 100 kHz). A total of 256 acquisitions were enough to obtain a good signal-to-noise ratio. The spectra were deconvolved in Gaussian−Lorentzian components by means of the program WINNMR (Bruker).

Leaching tests were run for a 0.1 cm^{-1} glass surface/water volume ratio. After washing with acetone, each sample, shaped as a glass slice with an area in the range of 1−6 cm^2, was immersed in a polyethylene test bottle containing bidistilled water and kept suspended. The test temperature was 37 °C; withdrawals were made after 5 h for two different samples for each measurement. After the leaching time indicated above the solutions were tested by inductively coupled plasma (ICP Spectroflame D, Varian) for determining the Na, Ca, Si, Zn, and P contents. The data were computed as grams per unit of surface area to get comparable results.

Scanning electron microscopy (SEM, Philips PSEM 500 XL-40) and energy-dispersive spectrometry (EDS; X-EDS Edax PV9900) techniques were performed on the glasses before and after the soaking in SBF solution for analyzing the morphological and compositional changes of their surface.

Transmission electron microscopy (TEM, JEM 2010 JEOL) was performed on the glasses after SBF soaking to better define and characterize the formation of crystalline phases.

The SBF was prepared according to Kokubo et al.[13] with the ion concentration and pH close to those of human blood plasma. A constant powder mass/liquid volume (0.25 g/50 mL) ratio was maintained, and the soaking was carried out at 37 °C, under continuous stirring and for various time intervals (10 h and 4, 15, and 30 days).

Computational Procedure. The input structures for the glass compositions experimentally characterized in this work were obtained by adding randomly the appropriate number and type of atoms into the simulation box of around 25 Å edge length. Periodic boundary conditions were applied to the cubic boxes containing, on average, 1400 atoms. The starting volume of the system was expanded by up to 30% to account for the estimated thermal expansion coefficient and then scaled to reproduce the experimental density at the final simulation temperature.

The annealing protocol used was optimized and described exhaustively in a previous work where zinc soda-lime glasses were studied.[5] Input structures were melted at nominal temperatures of 12 000 K, and the quenching scheme used to bring

TABLE 2: Parameters Used for the Four-Range Buckingham Potential

pair	A (eV)	ρ (Å)	C (eV Å^{-6})	ref
O−O	3.1161×10^6	0.1515	61.3916	15
Si−O	1036.9	0.3259	0.0	15
Na−O	1226.8	0.3065	0.0	15
Ca−O	1228.9	0.3118	0.0	15
Zn−O	700.3	0.3372	0.0	16
P−O	1273.4	0.3227	0.0	17

the system to 300 K corresponds to a cooling rate of approximately 4.6×10^{13} K/s. A time step of 2 fs was used. The long-range electrostatic potential was evaluated by the Ewald summation method with the cutoff distance set at 12 Å and precision set to 10^{-6}. The short-range cutoff distance was set at 7.6 Å.

As usual, in the Born model, the ions were treated as point charges with short-range forces acting between them. The short-range interactions between Si−O, Zn−O, P−O, Na−O, and Ca−O were modeled by a four-range Buckingham potential: $U(r) = A[\exp(-r/\rho)] - (C/r^6)$, where $U(r)$ is the short-range potential energy between pairs with a separation of r. The parameters A, ρ, and C are listed in Table 2.

The Si−O, Na−O, Ca−O, and O−O interactions were taken from Vessal,[14] as used by Cormack and Cao.[15] The Zn−O interaction parameters were taken from Lewis and Catlow.[16] Several P−O parameters available in the literature[16] were tested in preliminary simulations on the HP5, HP8, and HP5Z5 systems, and the suitability of the parameters finally chosen[17,18] was judged on the basis of the agreement of the average values observed from the simulations for bond lengths, bond angles, and coordination numbers (CNs) with respect to X-ray data of crystalline phosphates.

All the simulations were conducted applying a three-body screened Vessal potential[14] to the O−Si−O bond angle. A rigid ion model was adopted; that is, no explicit account of electronic polarization ability was included. Data collection was performed every 50 time steps during the last 10 000 time steps of the whole MD run.

MD simulations were performed with the DL_POLY[19] program, using Cerius2[20] as a graphical interface.

Results and Discussion

The ZnO maximum content added to H that enables a homogeneous glass to be obtained, (HZ20), is 15.9 mol % (corresponding to 20.0 wt %). Further ZnO addition gives rise to an opaque material, although a longer soaking time (6 h) at 1600 °C and a very fast quenching are applied. On average the molar ratio $SiO_2/Na_2O/CaO/P_2O_5$ in the H series is 19:10:11:1 corresponding to $(2 - y)SiO_2 \cdot 1Na_2O \cdot 1.1CaO \cdot yP_2O_5 \cdot xZnO$ with $x = 0$, 0.16, 0.35, 0.78 and $y = 0.10$, independently on ZnO addition; for the HP5 and HP5Z5 glasses the molar ratio is 18:10:11:2 corresponding to $(2 - y)SiO_2 \cdot 1Na_2O \cdot 1.1CaO \cdot yP_2O_5 \cdot xZnO$ with $x = 0$, 0.16 and $y = 0.20$. P_2O_5 favors the dissolution of ZnO in the glass; in fact, the maximum concentration of ZnO allowed in the glass of composition $Na_2O \cdot CaO \cdot 2SiO_2$ is 14.5 mol %.[5]

Density. The density values measured for the series of glasses studied are reported in Table 3. In the series of the HZ glasses density increases linearly with Zn concentration ($r = 0.999$, slope = 0.022) suggesting a unique structural role of Zn in the glass network in the range of concentrations allowed. The semiempirical method derived by Appen[21] to predict the density on the basis of additivity of the contributions due to each oxide in the glass gives rise to a straight line ($r = 0.999$, slope = 0.020). The discrepancy in the slope of the two linear regressions highlights the weakness of the additivity approximation in this series of glasses and can be ascribed to the change in the molar volume term of the oxides.

TABLE 3: Experimental and Calculated[21] Density Values (g/cm^3)

glass	experimental (±0.002)	calculated
H	2.719	2.719
HZ5	2.815	2.791
HZ10	2.900	2.867
HZ20	3.075	3.031
HP5	2.721	2.715
HP8[a]	2.772	2.709
HP5Z5	2.808	2.787

[a] Partially crystallized.

TABLE 4: Glass-Transition (T_g), Crystallization (T_c), and Melting (T_m) Temperatures and Tentative Assignments of the Crystallization Peaks

		$T_c \pm 2$ °C			
glass	$T_g \pm 2$ °C	$Na_2CaSi_2O_6$	$Na_4Zn_2Si_3O_{10}$	β-$NaCaPO_4$	$T_m \pm 2$ °C
H	521	707			1190
HZ5	493	693			1135
HZ10	483	683			1026
HZ20	490	655	624, 590[a]		1024
HP5	516	684		634	1172
HP5Z5	498	656	632		1152
HP8[b]	498	693			671

[a] Could be assigned also to the Zn_2SiO_4 crystallization. [b] Partially crystallized.

The substitution of P_2O_5 for SiO_2 (H and HP5) does not change the density value significantly.

Thermal Analysis. Glass-transition (T_g), crystallization (T_c), and melting temperature (T_m) are summarized in Table 4. The maximum value of T_g is measured for the zinc-free H glass. The T_g value decreases by increasing the P_2O_5 content (HP5) and the ZnO content. The H glass presents also the maximum of T_c and T_m whose values decrease along the whole series. The behavior of T_g suggests that the addition of ZnO results in a weakening of the glass network and a decreasing of the glass viscosity up to 7.8 mol % of ZnO; afterward, the effect seems to be reversed. This dual trend has been confirmed by preparing and testing a glass with an intermediate concentration of ZnO HZ15 (12.9 mol %; $T_g = 488$ °C, data not reported in Table 4).

Otherwise, the temperature of the first crystallization peak decreases continuously by increasing the ZnO concentration.

Powder XRD. The XRD of the as-quenched samples is characteristic of soda-lime phosphosilicate glasses. An exception is HP8, whose pattern, in addition to the broad peaks centered at 2.81−2.83 Å, displays sharp peaks suggesting that partial crystallization has occurred.

The XRD patterns of the same powder obtained after glass crystallization at a temperature corresponding to the first T_c peak differ one to another for number and position of the peaks, and in addition, the counts and relative intensity of each peak depend on the crystallization time, 2 h and 30 min or 5 h (see Table 5). The ternary sodium−calcium−silicate $Na_2CaSi_2O_6$[25] is identified as the main phase in the XRD patterns of H and HZ5, no matter what the crystallization time is. β-$NaCaPO_4$[26] is identified in H only after 5 h of crystallization.

$Na_4Zn_2Si_3O_{10}$[27] becomes the main phase in the HZ10 and HZ20 XRD patterns; Zn_2SiO_4[28] is also identified in these glasses as a minor phase.

In the HP5 and HP5Z5 glasses, a 2 h and 30 min long crystallization yields $Na_2CaSi_2O_6$ as the main phase. The

TABLE 5: (a) Crystal Phases, Relative Intensity (I/I_0), and Counts of the Principal Peak Identified by XRD Analysis after Two Different Thermal Treatments of Length t_c and (b) Structural Parameters of the Crystal Phases Obtained by Glass Crystallization

(a) Crystal Phases, Relative Intensity (I/I_0), and Counts of the Principal Peak

		t_c = 2 h and 30 min		t_c = 5 h	
glass	crystal phase	I/I_0 (%)	counts	I/I_0 (%)	counts
H	$Na_2CaSi_2O_6$	100	5013	100.0	16 435
	β-$NaCaPO_4$			2.3	773
HZ5	$Na_2CaSi_2O_6$	100.0	3434	100.0	13 197
	$Na_4Zn_2Si_3O_{10}$	46.1	1584	29.7	3919
	Zn_2SiO_4	4.1	139	5.1	671
HZ10	$Na_4Zn_2Si_3O_{10}$	100.0	4928		
	$Na_2CaSi_2O_6$	55.3	2725		
	Zn_2SiO_4	3.1	154		
HZ20	$Na_4Zn_2Si_3O_{10}$	100.0	9643	100.0	22 771
	$Na_2CaSi_2O_6$	14.2	1369	35.7	8136
	Zn_2SiO_4	6.5	625	18.3	4160
HP5	$Na_2CaSi_2O_6$	100.0	3422		
	β-$NaCaPO_4$	17.4	595		
HP5Z5	$Na_2CaSi_2O_6$	100.0	3080		
	β-$NaCaPO_4$	18.5	571		
	$Na_4Zn_2Si_3O_{10}$	18.4	566		
HP8	β-$NaCaPO_4$	100.0[a]	3174[a]	69.6	8046
	$Na_2CaSi_2O_6$			50.0	5788

(b) Structural Parameters

	M−O average bond length (Å)					M average CN				
crystal phase	Si−O	P−O	Ca−O	Na−O	Zn−O	Si	P	Ca	Na	Zn
$Na_2CaSi_2O_6$[5,22]	1.60		2.41	2.56		4		5.0	6.5	
β-$NaCaPO_4$[23]		1.54	2.47	2.54			4	7.7	5.3	
Zn_2SiO_4[24]	1.63				1.97	4				4

[a] XRD analysis on as-quenched material.

increase of the P_2O_5 content up to 8.7 mol % gives rise, also after a very fast quenching (HP8), to an opaque material whose XRD pattern reveals the presence of β-$NaCaPO_4$; after 5 h of crystallization $Na_2CaSi_2O_6$ is also identified.

In the series of glasses $Na_2O{\cdot}CaO{\cdot}2SiO_2{\cdot}xZnO$ ($x = 0-0.68$) the crystallization (2 h and 30 min) of the first term, $x = 0$, led to $Na_2CaSi_2O_6$, whose formula corresponds to the molar ratio among reagent oxides. In the same series $Na_4Zn_2Si_3O_{10}$ (for $x = 0.17$ and 0.34) and Na_2ZnSiO_4 (for $x = 0.68$) could also be identified.[5]

In the present series, the thermal treatment length (2 h and 30 min or 5 h) influences proportionally the counts of the main peak of all phases, but the relative intensity values might have a different trend. In HZ20 the lengthening of the thermal treatment increases both the I/I_0% of $Na_2CaSi_2O_6$ and Zn_2SiO_4 and the counts of all the crystal phases present, with the greatest increase in counts shown by $Na_2CaSi_2O_6$ and Zn_2SiO_4. This suggests that Zn_2SiO_4 is mainly formed by transformation of $Na_4Zn_2Si_3O_{10}$. This releases silica and sodium oxide which afterward can react with CaO forming $Na_2CaSi_2O_6$. The same behavior is observed for the HZ5 glass: the relative intensity of the $Na_4Zn_2Si_3O_{10}$ signal decreases from 46.1 to 29.7%, while that of Zn_2SiO_4 increases from 4.1 to 5.1%.

Crystal Structure Description. All crystal structures of the compounds formed during glass crystallization are known except that of $Na_4Zn_2Si_3O_{10}$; nevertheless, this is described in the literature[5] as a three-dimensional polymer with a β-cristobalite type arrangement and both silicon and zinc present at tetrahedral coordination geometry. In the solid-solution series $Na_{6-2x}Ca_{3+x}Si_6O_{18}$ ($0 \le x \le 1$), the extreme $x = 0$ value corresponds to $Na_2CaSi_2O_6$ and $x = 1$ corresponds to $Na_2Ca_2Si_3O_9$. The structure of $Na_2CaSi_2O_6$ consists of puckered $[Si_6O_{18}]^{6-}$ rings held together by oxygens bonded to cations. The rings are symmetrical and stacked along the c axis while the cations are distributed in four different sites with distorted coordination geometry and CN in the range of 4−8 for Na and 4−6 for Ca, respectively. The mean CNs obtained are 6.5 and 5.0 for Na^+ and Ca^{2+}, respectively. The cations are bonded to both bridging and nonbridging oxygens (NBOs).[5]

β-$NaCaPO_4$ is formed by two types of strings running along the a axis. String A consists of alternating Na atoms and discrete PO_4 tetrahedra; string B is made up by Ca atoms. The oxygens of the PO_4 tetrahedron are bonded to all the crystallographically independent cations so the crystal packing is built up by electrostatic interactions. Each oxygen of a PO_4 unit is coordinated to two to five cations, and, in addition, longer interactions are formed. Differently from the previously described silicates, the CN of the Na^+ ion is smaller that of Ca^{2+}.[23]

Zn_2SiO_4 is formed by the repetition, along the c axis, of two ZnO_4 tetrahedra alternating with one SiO_4 tetrahedron. The polymeric chains are connected by bridging oxygens (BOs) giving rise to a three-dimensional polymeric network; each oxygen atom is bonded to the two zinc atoms and to silicon and can be classified as three-bridging oxygens (TBOs).[24]

These results indicate that the phosphate group preferentially binds Na^+ and Ca^{2+} ions, while the silicate group does not show any preference toward cations. A second distinctive feature of the silicate group is its tendency to form polymeric arrangements; on the contrary the packing of phosphate is due to isolated groups surrounded by cations; therefore, in the crystalline state phosphate oxygens are only NBOs. The different binding modes between silicate and phosphate ions, when simultaneously present, can explain the negative effect of phosphate addition to silicate glass toward the formation of a glassy material with respect to a crystalline one. At increasing zinc content the XRD spectrum does not allow the identification of β-$NaCaPO_4$ even after an isothermal treatment 5 h long. This indicates that silicate crystallization is facilitated with respect to the phosphate one. A possible explanation is that the silicate group bears a more negative charge that exerts a more pronounced sequestering ability toward cations with respect to phosphate. On the basis of the XRD results and thermal parameters we can tentatively assign the crystallization peaks as reported in Table 4.

^{29}Si and ^{31}P MAS NMR Spectra. MAS NMR spectra are determined on the Zn-containing H glass series to investigate the medium range order (Q^n distribution) of the glass network formed by Si, P, and Zn. Figure 1a shows the ^{29}Si MAS NMR spectra of glasses H, HZ5, HZ10, HZ20, HP5, and HP8.

All the spectra appear quite featureless, and their deconvolution is not easy. Tentative Gaussian fits are reported in Table 6. The spectrum of sample H has been deconvolved in two peaks at −80 and −87 ppm, which can be assigned to Q^2 and Q^3 structural units, respectively.[29] The addition of ZnO to the silica matrix determines a shift of the center of mass of the spectrum toward the paramagnetic direction (low field). Rather than calling for a progressive depolymerization of the glass ($Q^n \rightarrow Q^{n-1}$), we assign this downfield shift to the formation of Si−O−Zn structural units [Q^n(Zn)]. As a matter of fact, a simple electrostatic model[30] shows that the substitution of Zn for Si in a Q^n unit causes the chemical shift to decrease about 10%, in agreement with the tentative assignments of the structural units of the glasses HZ10 and HZ20 reported in Table 6.

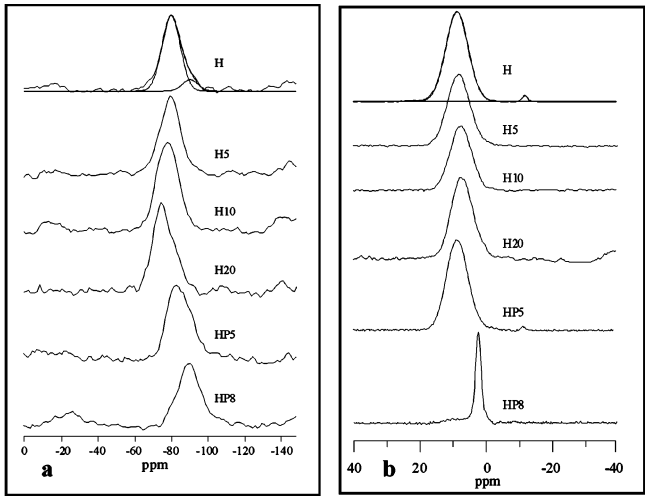

Figure 1. ^{29}Si (a) and ^{31}P (b) MAS NMR spectra of glasses H, HZ5, HZ10, HZ20, HP5, and HP8.

The number of Q^2 units seems to increase at the expenses of Q^3 passing from HZ10 to HZ20, in contrast with the trend detected passing from H to HZ5 and to HZ10. This apparent disagreement in the trend can be rationalized by invoking the formation of Q^3(2Zn) structural units [$Q^3(2Zn) = Q_{Si}^3$ linked to two ZnO_4 and to one SiO_4 tetrahedra], which could be characterized by a chemical shift very close to that of the Q^2-(Zn) groups [$Q^2(Zn) = Q_{Si}^2$ linked to one ZnO_4 and to one SiO_4 tetrahedra). Finally, the increase of P_2O_5 determines a shift to upfield of the bands, which corresponds to a higher polymerization of the glasses (or glass−ceramics). From the areas of the different components we obtain the percentage of BOs and NBO listed in Table 6a, by assuming that the contribution of each component is equally partitioned between the n BOs of the corresponding Q^n unit.

Figure 1b shows the ^{31}P MAS NMR spectra of the same samples. All the glassy samples display a main peak at about 8 ppm that is attributed to monophosphate (Q^0) units.[31]

The small peak observed at −12 ppm in the samples H and HP5 is likely due to Q^2 (chains or rings) units. The addition of ZnO causes the progressive increase of a shoulder at ∼2 ppm that is assigned to diphosphate units. Table 6 reports the Gaussian fits of the spectra.

The glass−ceramic sample HP8 shows a narrow peak at about 3 ppm and a weak and broad feature at 8 ppm that can be attributed to PO_4^{3-} units in the crystalline and glassy phases, respectively, in agreement with our X-ray measurements that show (after crystallization) the formation of the phase β-$NaCaPO_4$. A careful analysis of the spectrum also evidences the presence of diphosphate units (see Table 6) in the Zn-free glass.

UV−Vis Spectroscopy. Information on the coordination geometry of Zn^{2+} can be obtained by UV−vis on materials where Co^{2+} replaces Zn^{2+}, because Co^{2+} (d^7 electronic configuration) is isomorphous with Zn^{2+}.[32] Therefore, cobalt(II)-containing glasses have been prepared as the probe of the corresponding zinc-containing glasses (HZ series). Literature data on Co^{2+}-containing glasses concerning sodium borate glasses at a very low cobalt content show that the octahedral geometry is observed at low sodium concentration (absorption maximum at 550 nm), and the tetrahedral one is at higher sodium content (absorption maxima at 512, 582, and 626 nm).[33] Therefore, a tetrahedral geometry is expected in the series of glasses studied because the Na_2O percentage is greater than 20%. The electronic spectra of HCo5 and HCo10 are superimposable, and the absorbance increases with increasing of the Co content. As expected the spectra are similar to the literature spectrum of a glass containing tetrahedrally coordinated Co^{II} ion (absorption maxima at 524, 587, and 634 nm),[34] the main difference being the shift toward high λ values observed for our glasses with respect to the reference one. This finding corroborates the previous results obtained by the combined experimental and computational study on the quaternary glass system $Na_2O{\cdot}CaO{\cdot}SiO_2{\cdot}ZnO$,[5,35,36] where Zn was invariantly found in a tetrahedral geometry across the entire range of concentrations investigated.

Chemical Durability in Bi-Distilled Water of Glass Sheets. The concentration (ppm) of species detected in water after 5 h of immersion is reported in Table 7. All examined glasses present the same surface glass to water volume ratio (0.1 cm^{-1}). For a better understanding of the chemical durability behavior in water we have calculated the leaching percentage (wt %) for each constituent of the glasses (Table 7). Zn addition causes a global reduction of ion leaching, and for HZ20 the detected concentrations of silicon, phosphate, and zinc are very close to the detection limit of the instrument. On the contrary the increase in the P_2O_5 content in the glass gives rise to a lower chemical durability; in fact, for the HP5 glass we have found a sharp increment of Si and Na leaching.

This result suggests that the increment of P_2O_5 content is able to compensate the effect of Zn addition on the chemical durability. The opposite effects on chemical durability of ZnO and P_2O_5 addition balance each other in the HP5Z5 glass whose behavior in solution is similar to that of the H glass.

Characterization of the HP5Z5 Surface after SBF Soaking. Preliminary studies on the initial stages of the HP5Z5 in vitro bioactivity reveal similarities with the well documented behavior of Bioglass 45S5.[2] After 30 days of soaking in SBF, SEM/EDS studies distinguish different superimposed layers; the internal layer is constituted essentially of silicon and oxygen, while in the most external layer high concentrations of calcium, phosphorus, and zinc are found. The corresponding XRD pattern reveals two phosphatic phases: the zinc-containing phase, $CaZn_2(PO_4)_2{\cdot}2H_2O$,[37] and the hydroxiapatite, $Ca_{10}(PO_4)_6(OH)_2$.[37]

Moreover, TEM/EDS morphological studies carried out in the same experimental conditions confirm the presence of crystalline particles, constituted by Ca, P, and Zn, dispersed in an amorphous matrix that can be assigned to the above-mentioned zinc-containing phase.

MD Simulations. The force field used for the Zn atom has been validated previously for the quaternary glass system $Na_2O{\cdot}CaO{\cdot}SiO_2{\cdot}ZnO$.[5,35,36] A test of the reliability of the parametrization used in this study for the P atom is provided by the comparison of the short-range structure observed from the simulation with the one experimentally determined. Table 8 lists distances, angles, and CNs determined for the β-$NaCaPO_4$ phase obtained from crystallization of our glasses and for vitreous and crystal phosphate phases taken from literature,[38−42] together with the results of the simulations.

Inspection of Table 8 shows that, in general, structural properties are reproduced reasonably well, the major discrepancy being found for the P−O−P angle, the value of which is statistically scarcely significant because the number of bridged PO_4 tetrahedra in the glasses studied is extremely low.

Therefore, while it is likely that a more accurate parametrization would be necessary to reproduce experimental thermodynamics parameters,[43] a simple force field, which includes only the two-bonded interaction terms and formal charges, seems to be sufficiently adequate to derive structural descriptors to be

TABLE 6: Gaussian Components of the Line Shape[a]

(a) ^{29}Si MAS NMR

	component 1				component 2				component 3					
glass	CS (ppm)	area (%)	fwhh (ppm)	unit	CS (ppm)	area (%)	fwhh (ppm)	unit	CS (ppm)	area (%)	fwhh (ppm)	unit	BO (%)	NBO (%)
H	−80	94	5.0	Q^2	−87	6	11.1	Q^3					51.5	48.5
HZ5	−80	63	5.4	Q^2	−86	37	11.4	Q^3(Zn)					59	41
HZ10	−74	44	8.3	Q^2(Zn)	−80	45	7.9	Q^3(Zn)	−85	11	6.3	Q^3	64	36
HZ20	−74	81	10.4	Q^2(Zn)	−81	10	4.5	Q^3(Zn)	−85	9	4.2	Q^3	71	29
HP5	−82	89	13.8	Q^2	−88	4	3.7	Q^3	−91	7	3.7	Q^3	53	47
HP5Z5	−81	88	11.2	Q^2	−89	12	4.5	Q^3					53	47
HP8	−80	12	6.3	Q^2	−89	76	12.3	Q^3	−98	12	7.9	Q^3	72	28

(b) ^{31}P MAS NMR

	component 1			component 2			component 3			crystalline		
glass	CS (ppm)	area (%)	fwhh (ppm)	CS (ppm)	area (%)	fwhh (ppm)	CS (ppm)	area (%)	fwhh (ppm)	CS (ppm)	area (%)	fwhh (ppm)
H	8.7	94	8.2				−11.8	6	4.1			
HZ5	8.4	98	8.0	1.3	2	5.1						
HZ10	7.7	94	7.4	2.2	6	5.3						
HZ20	7.1	81	6.8	2.9	19	5.7						
HP5	8.5	90	9.2	2.1	7	4.9	−12.0	3	4.0			
HP5Z5	7.8	100	9.0									
HP8	7.8	4	9.2	1.4	4	5.1				2.4	92	2.6

[a] Abbreviations: CS, chemical shift; fwwh, full width at half-height; unit, hypothesized structural unit.

TABLE 7: Concentrations (ppm), Leaching Percent of Glass Constituents X_i, and Percent Total Leaching ($\sum\%X_i$) in Bidistilled Water after 5 h of Immersion of the Investigated Glasses[a]

	Si		Na		Ca		PO_4		Zn		
glass	ppm ± 0.1	% Si ± 0.01	ppm ± 0.1	% Na ± 0.01	ppm ± 0.1	% Ca ± 0.01	ppm ± 0.1	% P ± 0.01	ppm ± 0.1	% Zn ± 0.02	$\sum\%X_i$ ± 0.06
H	2.4	0.08	3.2	0.13	4.0	0.17	1.1	0.31			0.69
HZ5	0.7	0.02	2.7	0.11	4.2	0.18	0.8	0.23	0.2	0.04	0.54
HZ10	1.1	0.04	1.6	0.07	2.2	0.10	0.4	0.12	0.5	0.04	0.33
HZ20	0.1	0.00	0.9	0.04	0.7	0.03	0.1	0.03	0.2	0.01	0.10
HP5	6.8[b]	0.26	5.5	0.23	3.6	0.16	1.7	0.26			0.91[c]
HP5Z5	1.5	0.06	3.5	0.15	3.8	0.17	1.5	0.24	0.4	0.07	0.62
HP8	3.0	0.10	4.7	0.18	5.1	0.20	5.6	0.41			0.89

[a] Charges are omitted. [b] err ± 0.3. [c] err ± 0.08.

TABLE 8: Comparison between the MD and the Experimental Data for the P in Tetrahedral Geometry

	P−O (Å)					
phase	average	P−NBO	P−BO	P−O−P (deg)	O−P−O (deg)	notes
P_2O_5	1.54	1.43	1.58	137	102[a] 118[c]	ref 38, *b*
P_2O_5−ZnO		1.47	1.62			ref 39, *b*
β-$NaCaPO_4$	1.54	1.48−1.61			109.4	ref 23, *d*
SiP_2O_7	1.53		1.51−1.59	139	109.4	ref 40, *e*
$Zn(PO_3)_2$	1.53	1.45−1.50	1.55−1.62	136	103[a] 109[c] 119[g]	ref 41, *f*
$NaPO_3$	1.54	1.48−1.50	1.59−1.60	135	102[a] 109[c] 120[g]	ref 42, *f*
MD	1.51	1.50	1.60	146 125−160[h]	109 104−116[h]	

[a] BO−P−BO. [b] Vitreous forms. [c] NBO−P−BO. [d] Isolated PO_4 tetrahedra. [e] P_2O_7 units. [f] One-dimensional polymer. [g] NBO−P−NBO. [h] Center and width at half-maximum of the distribution.

related to the variation of chemical physics properties as a function of glass composition.

Thus, in our study the results of MD simulations constitute the basis for a QSPR analysis that allows for interpretation and, hopefully, prediction of experimental data. The values of some physically meaningful descriptors derived from MD simulations which correlate with experimental data we have measured on these glasses are listed in Table 9. In particular, (a) N^0_{X-O-X}/O_{tot} is the total number of Si−O−Si, Si−O−Zn, Si−O−P, P−O−Zn, and Zn−O−Zn bridges found in the simulated glasses normalized for the total number of oxygen atoms (O_{tot}). This is an overall descriptor of the degree of polymerization of the glass network. (b) N^0_{Si-O-X}/O_{tot} is the number of Si−O−Si, Si−O−Zn, and Si−O−P found in the simulated glasses normalized for O_{tot}. (c) $F_{network}$ is the overall strength of the network computed as the sum of the X−O bond energy

TABLE 9: Selected Structural Descriptors Derived from MD Simulations

glass	Si−O−Si N^0	Si−O−P N^0	Si−O−Zn N^0	P−O−Zn N^0	Zn−O−Zn N^0	P−NBO (%)	Na−NBO (%)	Ca−NBO (%)	Si−O−X N^0	X−O−X N^0	O_{tot} N^0	N^0_{Si-O-X}/O_{tot}	N^0_{X-O-X}/O_{tot}	$F_{network}$ (kcal/mol)
H	197	10	0	0	0	87	73	95	207	207	732	0.28	0.28	838
HZ5	204	10	71	5	3	86	67	88	285	293	751	0.38	0.39	710
HZ10	178	12	148	17	6	70	61	80	338	361	772	0.44	0.47	611
HZ20	155	8	283	34	58	57	51	70	446	538	813	0.55	0.66	500
HP5	206	31	0	0	0	83	74	95	237	237	767	0.31	0.31	821
HP5Z5	201	21	59	20	2	79	68	88	281	303	784	0.36	0.39	704
HP8	190	77	0	0	0	78	80	93	267	267.	819	0.33	0.33	789

TABLE 10: Correlation Matrix (*r* Values) of the Experimental Data and Theoretical Descriptors of the Seven Glasses Studied

	density	% BO (NMR)	T_g	T_c (1st peak)	% Na	% Ca	% P	$\sum$%X_i	% P−NBO	% Na−NBO	% Ca−NBO	N^0_{X-O-X}/O_{tot}	N^0_{Si-O-X}/O_{tot}	$F_{network}$
density	1.000													
% BO (NMR)	0.641	1.000												
T_g	−0.722	−0.656	1.000											
T_c (1st peak)	−0.870	−0.437	0.429	1.000										
% Na	−0.833	−0.432	0.659	0.538	1.000									
% Ca	−0.905	−0.426	0.465	0.820	0.747	1.000								
% P	−0.859	−0.223	0.551	0.750	0.768	0.924	1.000							
$\sum$%X	−0.922	−0.398	0.670	0.714	0.956	0.875	0.914	1.000						
%P−NBO	−0.935	−0.703	0.635	0.863	0.667	0.900	0.758	0.779	1.000					
%Na−NBO	−0.920	−0.310	0.600	0.797	0.860	0.921	0.977	0.970	0.792	1.000				
%Ca−NBO	−0.992	−0.577	0.743	0.840	0.859	0.917	0.902	0.951	0.918	0.950	1.000			
N^0_{X-O-X}/O_{tot}	0.996	0.598	−0.703	−0.895	−0.802	−0.914	−0.883	−0.914	−0.930	−0.932	−0.990	1.000		
N^0_{Si-O-X}/O_{tot}	0.992	0.629	−0.765	−0.846	−0.812	−0.895	−0.881	−0.915	−0.917	−0.925	−0.991	0.994	1.000	
$F_{network}$	−0.979	−0.566	0.804	0.822	0.844	0.872	0.892	0.939	0.894	0.938	0.993	−0.980	−0.988	1.000

multiplied by the number of X−O bonds in each bridge type and normalized for the total number of bridges (the X−O bond energy is derived from the dissociation energy of the XO_n oxide: 424 kcal/mol for SiO_2, 144 kcal/mol for ZnO, and 442 kcal/mol for P_2O_5);[44] (d) %P−NBO, %Na−NBO, and %Ca−NBO are the percentages of NBOs bonded to P, Na, and Ca ions.

The correlation matrix reported in Table 10 gives an overview of the collinearities existing between these descriptors for the whole series of seven glasses.

The variation in the density of the glasses studied is well described by all the descriptors considered; however, the best correlation is obtained by means of the N^0_{X-O-X}/O_{tot} descriptor (Figure 2a). The positive slope indicates that density increases with the overall packing degree of the atoms in the glasses obtained by adding Zn or substituting P for Si. It is worth noting that this descriptor allows the two series of glasses to be fitted in the same correlation.

The introduction of Zn in the network causes an increase in the polymerization because it manifests a clear preference to bond to BO atoms in a regular tetrahedral geometry in all the glasses studied. Moreover, in the HZ20 glass 5.6% of the TBOs associated to the Zn ion are observed in agreement with one of the phases separated upon crystallization of this glass, identified as willemite (Zn_2SiO_4), where all the oxygens are simultaneously bonded to two Zn atoms and one Si atom and, therefore, classified as TBO. The cross-linking gain is due to the formation of a number of Si−O−Zn, P−O−Zn, Si−O−P, and, at high Zn content, Zn−O−Zn bridges that overcome the reduction of the number of Si−O−Si bridges. These significant structural modifications observed in the simulated glasses upon Zn and P addition are supported by the ^{29}Si MAS NMR results. A good correlation is, in fact, observed between the experimental % of BO and the number of Si−O−X bridges (N^0_{Si-O-X}/O_{tot}) found in the simulated glasses (Figure 2b). It is worth noting that the standard error of the regression (s^2, in Figure 2) is below the error due to the spectra deconvolution scheme adopted (estimated approximately at 8%) and is essentially due to the HP5Z5 glass that, according to the simulation, undergoes a 4% increment in the amount of BO (57%) with respect to the parent HP5 glass (53%), which is not detected by the experiment.

An estimation of the percent of BO in the glass can be obtained merely from the glass compositional formula, but assumptions based on a preconceived notion of the glass structure are needed.[45] Thus, by assuming that Si and P play a traditional role in the glass, the percentages of BO computed for H and HP5 are 48.2 and 47.6, respectively. Moreover, by assuming a network former role for the zinc ion, 54.5, 61.2, 75.5, and 53.9 are the percentages of BO obtained for HZ5, HZ10, HZ20, and HP5Z5, respectively, whereas 47.1, 45.8, 43.2, and 46.6 are obtained by assuming a modifier role for the zinc ions. The discrepancy observed in the values computed making different assumptions argues for the advantages of using descriptors derived from molecular simulations in the QSPR approach.

Interesting is the behavior of the P atom which is preferentially found in isolated tetrahedral units (Q^0) surrounded by Na and Ca ions in the Zn-free glasses and is progressively included in the glass network by Zn addition (Figure 3). The P average Q^n found in the simulations ranges from 0.5 in the Zn-free glass to 1.78 in the HZ20 in agreement with the results of ^{31}P MAS NMR experiments.

The low tendency of the P ions to form mixed crystal phases with Si causes the formation of islets of different compositions into the glass structure; in particular, zones rich in Si, Na, and Ca and ones characterized by the presence of P, Na, and Ca can be observed in the simulated glasses. This is in good agreement with the crystal phases obtained from the H glass [β-$NaCaPO_4$ and $Na_2Ca(SiO_3)_2$], and it suggests that the crystal phases separated from glasses are reminiscent of the glass microstructure. This microsegregation phenomenon can explain the low solubility of P_2O_5 in H glasses; in fact, a molar concentration of 8.7% in P_2O_5 causes the precipitation of the

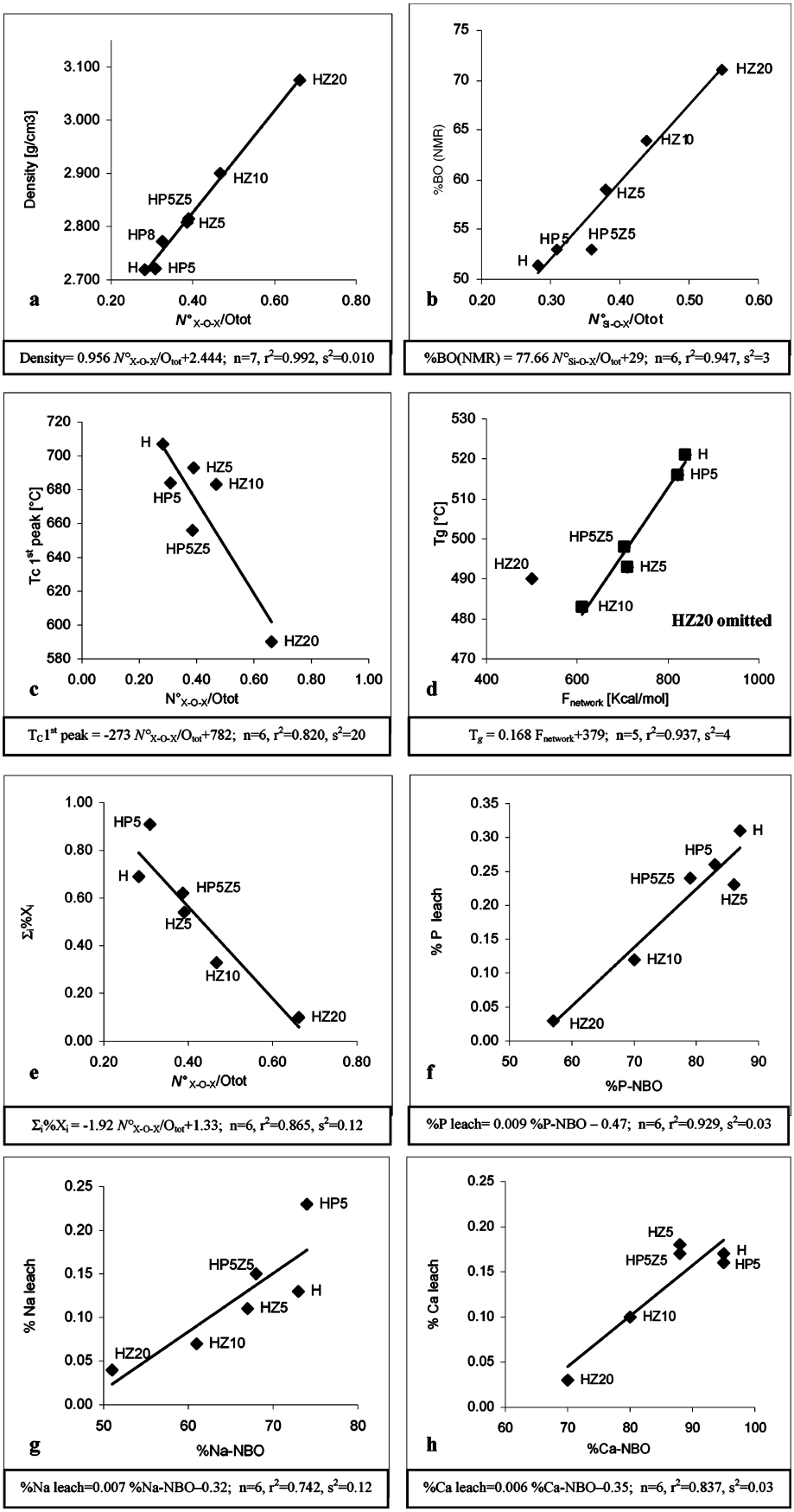

Figure 2. Correlations between structural descriptors and experimental data measured for the glasses studied. In graphs b−h HP8 is omitted because it is partially crystallized.

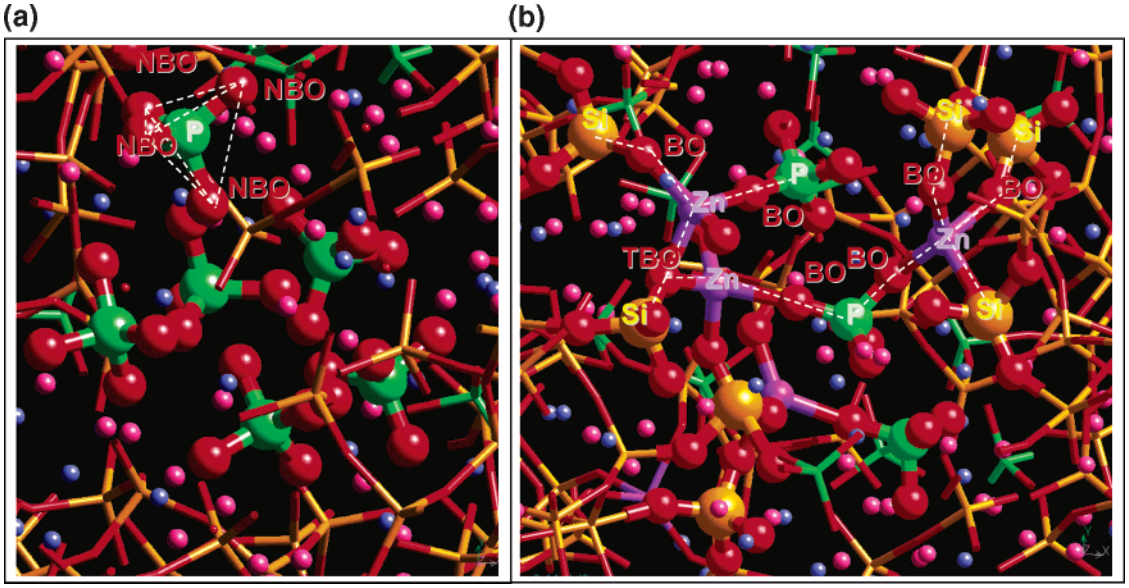

Figure 3. Snapshot of the simulated H (a) and HP5Z5 (b) glasses showing the zone rich in isolated P tetrahedra characteristic of H and the −Si−Zn−P−Zn− stings formed in HP5Z5. Si is represented in yellow, Zn in violet, P in green, O in red, Na in pink, and Ca in blue.

ortho-phosphate β-$NaCaPO_4$ in the HP8 system even with a fast cooling.

Although statistically poor, the correlation between the N^0_{X-O-X}/O_{tot} descriptor and T_c (first peak) provides interesting arguments (Figure 2c). The negative slope seems to suggest that the crystallization process would be favored by the complexation of the network, expressed by the total number of bridges formed. This trend can be partially understood by considering microsegregation as a pre-organization step which favors the crystallization process. Moreover, it has also to be considered that the Si−O−Zn, P−O−Zn, and Zn−O−Zn bridges newly formed involve bonds which are weaker with respect to the Si−O bonds in the $(Si-O-Si)_n$ chain. Therefore, while the degree of polymerization increases in the series of glass studied as a function of Zn addition, the strength of the overall network obtained decreases with respect to the one characteristic of the Zn-free glass. This is highlighted in Table 9, where the values of the $F_{network}$ descriptor are listed. $F_{network}$, encoding both structural and energetic properties of the network, is directly correlated (positive slope) to T_c (first peak) and explains the 68% of its variation. The reduction of the overall network strength by Zn addition is in line with the progressive decreasing observed for the T_g values measured for the HP5 and HZ series up to 15 mol % addition of Zn (Figure 2d). However, according to this model, the T_g value of HZ20 would be largely underestimated. Therefore, additional effects have to be considered to explain the nonlinear behavior which seems to dictate the variation of T_g as a function of Zn concentration. In fact, for example, the increment in the number of the X−O−X bridges detected in the series of simulated glasses can be achieved both by elongation of linear chains and by cross-linking between chains. The flexibility of the linear chains yields to low T_g, while the cross-linking reduces the ability of the polymer to twist and tangle resulting in T_g increasing.[7] The $F_{network}$ descriptor does not take into account explicitly the gain in cross-linking due to polymerization, which is indeed consistent in the HZ20 glass (Q^3 and Q^4 species contribute for more than 60% of the total Q_{Si} and Q_P species, respectively) and can overcome the loss in bond energy associates to the insertion of Zn and P in the −Si−O−Si− network.

The role of the network polymerization on the water chemical durability of the glasses is well-depicted by the relationship obtained between the total leaching ($\sum\%X_i$, sum of percent leaching of each constituent of the glasses) and the N^0_{X-O-X}/O_{tot} descriptor (Figure 2e). As expected, the reticulation effect of the Zn increases the glass durability by diminishing the concentration of ions leached by up to 1 order of magnitude with respect to the parent H glass. The degradation process is mainly regulated by the number of NBO species bonded to the P, Na, and Ca ions (Figure 2f−h), which ensure the presence of large channels for alkali migration in the network.

Conclusions

In this work the applicability of the quantitative structure−activity relationship approach for the rationalization and prediction of the technology-related properties of a series of complex multicomponent glasses has been tested for the first time. Notwithstanding that the validity of the approach has to be proved on a larger series and on various compositions to assess its general applicability, the results obtained are encouraging.

The statistical models obtained by making use of structural descriptors with high information content can be considered useful tools for exploiting and rationalizing the large amount of data derived by molecular simulations of the glasses and gaining further insight into the physical processes determining the properties of interest (interpretation). Moreover, interpolation of missing data can be attempted, with the prediction accuracy depending on the statistical robustness of the models.

Zn in the phosphosilicate glasses adopts a tetrahedral coordination, irrespective of its concentration, and copolymerizes with the Si tetrahedra causing an overall complexation of the network with respect to the parent H glass. A similar behavior was previously observed in our studies on soda-lime silicate glasses[5,35,36] and seems to be responsible for the chemical durability increment of the glasses.

The salient feature that emerges in this study is that Zn acts as a chaperon for the P insertion into the three-dimensional glass network. In fact, the P ion, which is usually found in isolated tetrahedra in Zn-free compositions, is progressively incorporated into the network as a function of zinc concentration. A highly ramified network of interconnected Si−Zn−P tetrahedra is thus formed, where segregation zones for the Ca ions are observed in close proximity to Si and P, whereas Na is almost uniformly

distributed. However, the Na ions associated as a charge compensator to ZnO_4 tetrahedra are strongly trapped in the network, and this contributes, together with the overall obstruction of the percolation channels due to the increase in the network ramification, to a drastic reduction in the overall leaching of the HZ20 glass.

An optimal ratio of Zn/P, to maintain bioactivity, is given by the HP5Z5 glass composition, in which the Na and Ca ions associated to Q_P^0 and Q_P^1 units find the percolation channel suitable for a rapid exchange with the H_3O^+.

Acknowledgment. This work was supported by Ministero dell'Università' e della Ricerca Scientifica e Tecnologica (MIUR, Grant 2003032158_005). The authors thanks Dr. Mauro Zapparoli (Centro Interdipartimentale Grandi Strumenti of Modena and Reggio E. University) for TEM measurements.

References and Notes

(1) Wilson, J.; Yli-Urpo, A.; Risto-Pekka, H. Bioactive glasses: clinical applications. In *An introduction to bioceramics*; Hench, L. L., Wilson, J., Eds.; Singapore: World Scientific, 1993; p 63.

(2) Hench, L. L. *J. Am. Ceram. Soc.* **1998**, *81* (7), 1705 and reference therein.

(3) Ito, A.; Kawamura, H.; Otsuka, M.; Ikeuchi, M.; Ohgushi, H.; Ishikawa, K.; Onuma, K.; Kanzaki, N.; Sogo, Y.; Ichinose, N. *Mater. Sci. Eng., C* **2002**, *22*, 21.

(4) Ennas, G.; Musinu, A.; Piccaluga, G.; Montenero, A.; Gnappi, G. *J. Non-Cryst. Solids* **1990**, *125*, 181.

(5) Lusvardi, G.; Malavasi, G.; Menabue, L.; Menziani, M. C. *J. Phys. Chem. B* **2002**, *106*, 9753.

(6) Montagne, L.; Palavit, G.; Delaval, R. *J. Non-Cryst. Solids* **1997**, *215*, 1.

(7) Karelson, M.; Lobanov, V. S.; Katritzky, A. R. *Chem. Rev.* **1996**, *96*, 1027.

(8) Katritzky, A. R.; Maran, U.; Lobanov, V. S.; Karelson, M. *J. Chem. Inf. Comput. Sci.* **2000**, *40*, 1.

(9) Tischendorf, B. C.; Alam, T. M.; Cygan, R. T.; Otaigbe, J. U. *J. Non-Cryst. Solids* **2003**, *316*, 261.

(10) Boiko, G. G.; Andreev, N. S.; Parkachev, A. V. *J. Non-Cryst. Solids* **1998**, *238*, 175.

(11) Sourial, E.; Peres, T.; Capobianco, J. A.; Speghini, A.; Bettinelli, M. *Phys. Chem. Chem. Phys.* **1999**, *1* (8), 2013.

(12) Cormack, A. N. Presented at X Conference of the Physics of Non-Crystalline Solids, Parma, Italy, 2003.

(13) Kokubo, T.; Kushitani, H.; Sakka, S.; Yamamuro, T. *J. Biomed. Mater. Res.* **1990**, *24*, 721.

(14) Vessal, B. *J. Non-Cryst. Solids* **1994**, *177*, 103.

(15) Cormack, A. N.; Cao, Y. *Mol. Eng.* **1996**, *6*, 183.

(16) Lewis, G. V.; Catlow, C. R. A. *J. Phys. C: Solid State Phys.* **1985**, *18*, 1149.

(17) Sauer, J.; Schroder, K. P.; Termath, V. *Collect. Czech. Chem. Commun.* **1998**, *63*, 1394.

(18) http://www.ri.ac.uk/potentials (accessed Feb 2005).

(19) Smith, W.; Forester, T. R. *J. Mol. Graphics* **1996**, *14*, 136.

(20) *Cerius2*; Accelrys, Inc.: San Diego, CA, 2001.

(21) Volf, M. B. *Mathematical Approach to Glass*; Glass Science and Technology 9; Elsevier: Prague, Czech Republic, 1988; references therein.

(22) Oshato, H.; Maki, I. *Acta Crystallogr., C* **1985**, *41*, 1575.

(23) Ben Amara, M.; Vlasse, M.; Le Flem, G.; Hagenmuller, P. *Acta Crystallogr., C* **1983**, *39*, 1483.

(24) www.MinCryst-Crystallographic Database for Mineral, 1877 CPDS cards. http://database.ien.ac.ru/mincryst (accessed June 4, 2004).

(25) www.MinCryst-Crystallographic Database for Mineral, 4882 CPDS cards. http://database.ien.ac.ru/mincryst (accesssed June 4, 2004).

(26) www.MinCryst-Crystallographic Database for Mineral, 2345 CPDS cards. http://database.ien.ac.ru/mincryst (accessed June 4, 2004).

(27) Powder Diffraction File, Inorganic Phases PDF N*o*. 37-409. JCPDS-ICDD: Swarthmore, PA, 1989.

(28) Powder Diffraction File, Inorganic Phases PDF N*o*. 37-1485. JCPDS-ICDD: Swarthmore, PA, 1989.

(29) Engelhardt, G.; Michel, D. *High-Resolution Solids State NMr of Silicate and Zeolites*; Wiley & Sons: Chichester, 1987.

(30) James, N.; Oldfield, J. *J. Am. Ceram. Soc.* **1985**, *107*, 6769.

(31) Grassaite, H.; Montagne, L.; Palavit, G.; Bernard, J. L. *J. Non-Cryst. Solids* **2000**, *263*−*264*, 312.

(32) Shannon, R. D. *Acta Crystallogr., A* **1976**, *32*, 751.

(33) Banford, C. R. *Colour Generation and Control in Glass*; Glass Science and Technology; Elsevier: New York, 1997; Vol. 2.

(34) *SciGlass 3.5, Universal System of Glass Properties*; SciVision: Burlington, MA, 1997.

(35) Lusvardi, G.; Malavasi, G.; Menabue, L.; Menziani, M. C.; *Adv. Sci. Technol.* **2003**, GVol. *1*, p 91. Ed. Techna srl, Faenza, Italy (ISBN 88-86538-38-3).

(36) Lusvardi, G.; Malavasi, G.; Menabue, L.; Menziani, M. C.; Segre, U.; Carnasciali, M. M.; Ubaldini, A. *J. Non-Cryst. Solids* **2004**, *710*, 345−346.

(37) *PCPDFWIN Version 2.3*; JCPDS (International Centre for Diffraction Data): Swarthmore, PA, 2002.

(38) Hoppe, U.; Walter, G.; Kronold, R.; Stachel, D. *J. Non-Cryst. Solids* **2000**, *263*−*264*, 29.

(39) Suzuya, K. *J. Non-Cryst. Solids* **1998**, *232*−*234*, 450.

(40) Bisset, V. G.; Liebau, F. *Acta Crystallogr., B* **1970**, *26*, 2233

(41) Averbuchi-Ponchot, P. M. T.; Durif, A.; Bagien-Beucher, H. *Acta Crystallogr., C* **1983**, *39*, 25.

(42) Jost, K. H. *Acta Crystallogr.* **1963**, *16*, 640.

(43) Liang, J. J.; Cygan, R. T.; Alam, T. M. *J. Non-Cryst. Solids* **2000**, *263*−*264*, 167.

(44) Varshneya, A. R. *Fundamentals of Inorganic Glasses*; Academic Press: USA, 1994.

(45) Klinowski, J.; Ramdas, S.; Thomas, J. M.; Fyfe, C. A.; Hartman, J. S. *J. Chem. Soc., Faraday Trans.* **1982**, *78*, 1025.